Bisphosphonate Inhibition of Phosphoglycerate Kinase: Quantitative Structure−Activity Relationship and Pharmacophore Modeling Investigation

Evangelia Kotsikorou,[†] Gurmukh Sahota,[‡] and Eric Oldfield*[,†,‡]

Department of Chemistry, 600 South Mathews Avenue, and Center for Biophysics and Computational Biology, 607 South Mathews Avenue, University of Illinois at Urbana−Champaign, Urbana, Illinois 61801

Received April 25, 2006

We report the results of a three-dimensional quantitative structure−activity relationship (3D-QSAR) and pharmacophore modeling investigation of the interaction of the enzyme 3-phosphoglycerate kinase (PGK) with aryl and alkyl bisphosphonates. For the human enzyme, the IC_{50} values are predicted within a factor of 2 over the 240× experimental range in activity, while for the yeast enzyme, binding of the more flexible alkyl bisphosphonates is predicted within a factor of ∼4 (over a 2500× range in activity). Pharmacophore models indicate the importance of two negative ionizable features, one hydrophobic feature, and one halogen feature, and docking studies indicate that bisphosphonates bind in a manner similar to the 3-phosphoglycerate molecule identified crystallographically. The results give a good account of the activities of a diverse range of bisphosphonate inhibitors and are of interest in the context of developing inhibitors of glycolysis in organisms that are totally reliant on glycolysis for ATP production, such as trypanosomatid parasites.

Introduction

The enzyme phosphoglycerate kinase (PGK,[a] EC 2.7.2.3) catalyzes the conversion of 1,3-bisphosphoglycerate and ADP into 3-phosphoglyceric acid (3-PGA) and ATP. In mammals,

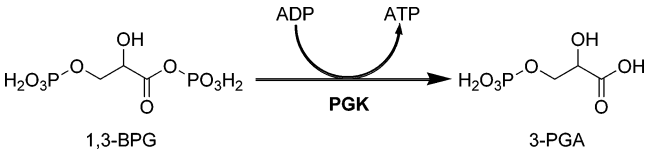

3-PGA is converted in several steps to pyruvate, which then enters the Krebs cycle, resulting in the production of large additional amounts of ATP. However, in many trypanosomatid parasites, such as *Trypanosoma brucei* (the causative agent of African sleeping sickness), *Trypanosoma cruzi* (the causative agent of Chagas disease), and *Leishmania* spp. (the causative agents of the leishmaniases), the latter enzymes are absent and, consequently, these organisms rely exclusively on glycolysis for energy (ATP) production. There is, therefore, considerable interest in the design of inhibitors of glycolysis as novel antiparasitic agents. To date, few such inhibitors have been reported,[1] but Bakker et al.[2,3] have created a detailed mathematical model of *T. brucei* glycolytic flux, based on the experimentally determined kinetic properties of all the enzymes involved in glycolysis, which points to PGK as being one of the more promising glycolytic enzyme targets for chemotherapeutic intervention,[3] since moderate inhibition of this enzyme can cause large changes in the glycolytic flux of the parasite while not affecting host red blood cells.

In addition to its potential importance as an antiparasitic drug target, inhibition of PGK in humans is expected to lead to accumulation of 1,3-bisphosphoglycerate and, via bisphosphoglycerate mutase, to increased levels of 2,3-bisphosphoglycerate. This is expected to result in decreased hemoglobin affinity for O_2,[4,5] resulting in enhanced O_2 release. Consequently, there is also interest in the development of PGK inhibitors for the treatment of cardiovascular disease.[6]

On the basis of the structure of the substrate 1,3-BPG, Blackburn and co-workers[7−9] have synthesized two series of PGK inhibitors in which the relatively labile phosphate groups are replaced by (nonhydrolyzable) phosphonate groups (containing P−C bonds). In some typical examples of the compounds they investigated, the electronegative oxygen atoms in 1,3-BPG

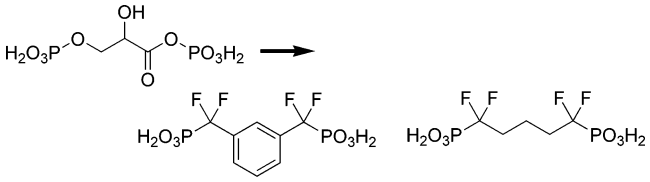

are replaced by highly electronegative but nonreactive (CF_2) groups and the backbone is replaced by an aryl or alkyl spacer. Substitution with halogens or hydroxyl groups in the α position (next to phosphorus) was used in an attempt to create isosteric and isopolar analogues of 1,3-BPG and also to probe the role of phosphonate acidity in protein binding.[10,11] The first series of compounds studied were relatively conformationally restrained, aromatic species, which were found to inhibit human PGK with IC_{50} values ranging from 0.84 to 200 μM.[7,9] The second series of analogues had more flexible alkyl or alkyl-substituted chains between the phosphonate centers, and their potencies (as determined by their dissociation constants against yeast PGK) ranged from 2 to 5000 μM.[8] However, there were no quantitative structure−activity relationship (QSAR) studies reported.

In our group, we have been interested in the development of several other classes of bisphosphonates for use as antiparasitic agents. The first group is the nitrogen-containing bisphosphonates, which inhibit the enzyme farnesyl diphosphate synthase (FPPS). We found that many of these compounds have

* Corresponding author: phone 217-333-3374; fax 217-244-0997; e-mail eo@chad.scs.uiuc.edu.
[†] Department of Chemistry.
[‡] Center for Biophysics and Computational Biology.

[a] Abbreviations: PGK, phosphoglycerate kinase; 3-PGA, 3-phosphoglyceric acid; 1,3-BPG, 1,3-bisphosphoglycerate; CoMFA, comparative molecular field analysis; CoMSIA, comparative molecular similarity indices analysis.

10.1021/jm0604833 CCC: $33.50
Published on Web 10/17/2006

considerable activity versus the trypanosomatid parasites[12−14] and we reported a series of 3D-QSAR (three-dimensional quantitative structure−activity relationship) and pharmacophore modeling investigations of cell growth and FPPS inhibition by these bisphosphonates,[15,16] work that later led to the development of other, novel FPPS inhibitors.[17] In addition, we recently reported QSAR investigations of another series of bisphosphonates that inhibit glycolysis (and cell growth) in *T. cruzi*, this time at the level of hexokinase.[18] It thus appeared to us to be of interest to see to what extent it might be possible to use these QSAR methods to predict the activities of the PGK/glycolysis bisphosphonate inhibitors reported previously, with the long-term goal of investigating their activity versus the trypanosomatid enzymes (and organisms), including the possibility of synergistic interactions in the glycolytic pathway with, for example, the hexokinase inhibitors.[18]

Computational Aspects

General Aspects. We used the methods of comparative molecular field analysis (CoMFA),[19] comparative molecular similarity indices analysis (CoMSIA),[20] and pharmacophore modeling.[21] The CoMFA method calculates interaction energies by use of electrostatic and steric probes at regularly spaced grid points and then correlates the variances in energies with the differences in activities. CoMSIA is a related method that replaces the distance terms in the Lennard-Jones and Coulomb-type potentials (in CoMFA), with Gaussian-type functions. A benefit of CoMSIA is that it is less sensitive to molecular alignment and provides useful graphical outputs correlating activity with structure. Pharmacophore modeling also correlates activities with the spatial arrangement of various chemical features and complements the CoMSIA approach. These 3D-QSAR methods have been used by us in previous work on bisphosphonates to generate models that are able to predict activities, typically within a factor of 2 over the range of activities observed.[15,16,18] Here, we first investigate the inhibition of human PGK by aromatic bisphosphonates, where IC_{50} values have been reported.[7,9] For human PGK inhibition we use as our definition of activity pIC_{50}, defined as

$$pIC_{50} = -\log [IC_{50}, M]$$

For the yeast PGK, IC_{50} values for enzyme inhibition were not reported. Rather, the dissociation constants (K_d) were determined, by an NMR method.[8] In this case, we use pK_d, defined as

$$pK_d = -\log [K_d, M]$$

The experimental errors reported (on average) for the two methods are 5% (for IC_{50}) and 28% (for K_d).[7−9]

3D-QSAR/CoMFA/CoMSIA. The structures of the bisphosphonate inhibitors investigated are shown in Figures 1 and 2 and were built and minimized with the Sybyl 7.0 Molecular Modeling program.[22] Energy minimization and geometry optimization by use of the Tripos force field was carried out for each molecule with a convergence criterion requiring a minimum RMS gradient of 0.01 kcal at a steepest descent step and 0.001 kcal at the following Powell[23] and Broyden, Fletcher, Goldfarb, and Shanno (BFGS)[24] steps. Structures were optimized to convergence at each minimization step. The atomic charges for the comparative molecular field analysis (CoMFA)[19] and comparative molecular similarity index analysis (CoMSIA)[20] calculations were determined by using the Gasteiger−Marsili[25] method. CoMFA fields and CoMSIA indices were calculated on a rectangular grid containing the aligned molecules. For CoMFA we used steric and electrostatic probes, while for CoMSIA we used electrostatic, steric, and acceptor probes. Hydrophobic and donor descriptors were not found to be beneficial in the calculations. The atomic coordinates of the models were then used to compute field values at each point of the 3D grid with a spacing of 2.00 Å. A partial least squares (PLS) analysis was then applied, to give the final QSAR correlation.

Pharmacophore Modeling. Pharmacophore modeling was carried out by use of the Catalyst[21] program. Initially, a conformational search was carried out with up to 256 conformations of each of the molecules, generated by using the "best quality" mode of ConFIRM. Then, the most active compounds were screened for a number of default functional groups (e.g., H-bond donor, positive ionizable, negative charge, hydrophobic) contained in Catalyst, together with a custom-made halogen feature (Catalyst does not have a default halogen feature). The functional groups that seemed to contribute most to activity were then selected and used to build a series of hypotheses with the HypoGen module in Catalyst, using default parameters. The hypotheses generated were then used to correlate activity with the functional groups present.

Docking Investigations. We used the AutoDock[26] program to dock selected bisphosphonates to the X-ray structure of *T. brucei* PGK,[27] basically using the parameters described previously.[28]

Results and Discussion

In this work, we investigate structure−activity relationships for aromatic bisphosphonates acting as inhibitors of the human PGK enzyme, as well as a second set of bisphosphonates, aliphatic species, binding to the yeast (*Saccharomyces cerevisiae*) enzyme. The sequences of the human and yeast enzymes are shown in Figure 3, together with, for comparison, the sequence of the *T. brucei* enzyme. There are clearly many highly conserved domains between the three sequences, corresponding to residues that contact the 1,3-BPG and ADP substrates, making it likely that structural (and SAR) results for one enzyme will be relevant to results for the other enzymes, just as is found, for example, in the structures of bisphosphonates bound to the FPPS enzymes from bacteria (*Escherichia coli*, *Staphylococcus aureus*),[29] *T. cruzi*,[30] and human.[31,32] Since the X-ray structures of pig[33] (99% identity, 100% similarity to humans) and *S. cerevisiae*,[34] as well as *T. brucei* PGK, have been reported to show considerable similarities, this opens up the future possibility of using structure-based design. But to begin with here, we focus on the use of (ligand-based) QSAR methods to predict the activities (IC_{50} and K_d values) of bisphosphonates binding to the human and *S. cerevisiae* enzymes, since these results are of interest in their own right, in addition to being of potential interest in the development of novel antiparasitic and cardiovascular agents.

Aromatic Bisphosphonates. We show in Figure 1 the structures of the 36 aromatic (and one olefinic) bisphosphonates whose activities in inhibiting human PGK were reported by Caplan et al.[7,9] The experimentally determined IC_{50} values of these compounds cover a 240× range in activity (from 0.84 to 200 μM) and for convenience are reproduced in Table 1, together with their corresponding pIC_{50} values. As noted previously,[7,9] it can be seen that α-substitution improves activity according to the following sequence: CH_2 (least potent) < CHOH < CCl_2 < CHCl ≅ CHF < CF_2 (most potent). α-Halogenation always improves activity, apparently because the resulting compounds are isosteric and isopolar with the natural substrate, 1,3-BPG. Ring methylation also enhances activity somewhat (compare, for example, compounds **27** and **37**), but nitrogen substitution of the ring (pyridyl instead of phenyl) decreases activity (e.g., compounds **3** and **9**). Finally, larger distances between the phosphonate groups (as compared to 1,3-BPG) have little effect on activity (e.g., **1** and **4**), but shorter distances appear to have a larger effect (**25**). To investigate these qualitative structure−activity relationships in more detail, we first used the CoMFA method. As described above, the molecules shown in Figure 1 were built and then geometry-optimized by using a three-step protocol consisting

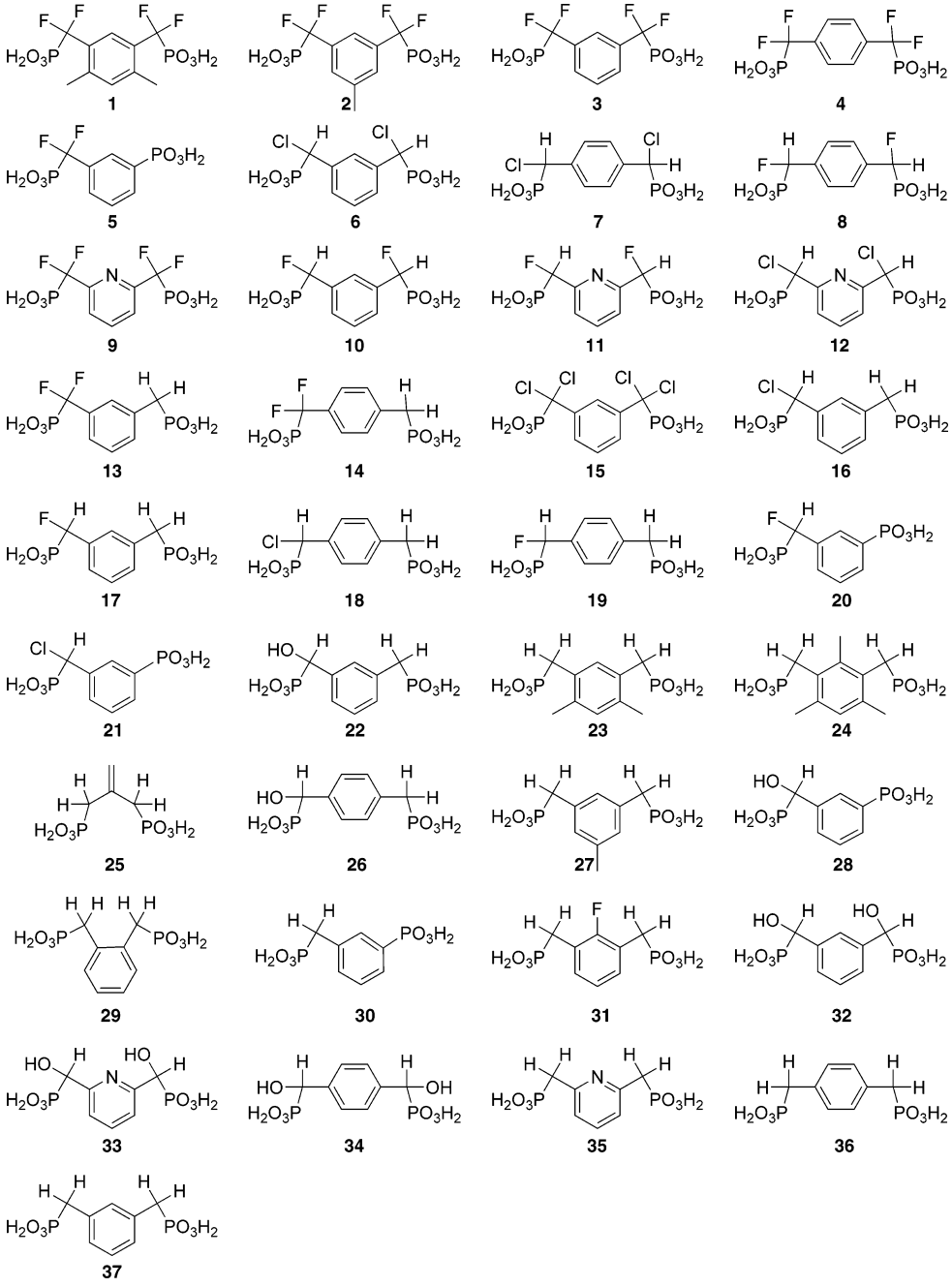

Figure 1. Structures of aromatic bisphosphonates investigated (rank ordered by decreasing activity).

of steepest-descent, Powell, and then BFGS algorithms, by use of the Tripos force field in the Sybyl 7.0 program.[22] Each minimized structure was then aligned, in three steps, by using the Database Align function in Sybyl 7.0. In the first step, molecules with four and five carbons between the phosphonate groups (except **29)** were aligned with the most active compound (**1**) as the shape reference. The atoms considered were those of the benzene ring (except the position that is substituted with nitrogen in **9**, **11**, **12**, **33**, and **35**), a phosphonate group, and its adjacent carbon. Next, compounds with six carbons between the phosphonate groups were aligned on the most active compound (**1**) by use of both phosphonate groups, their adjacent carbons, and four ring carbons. Finally, **25** and **29** were aligned by use of the phosphonate groups and their neighboring carbons, again with the most active compound (**1**) as the shape reference. The alignment is shown in Figure 4A. We used default settings to automatically build a three-dimensional rectangular grid with a 2.00 Å spacing, encompassing the alignment shown in Figure 4A, and then used steric and electrostatic probes to calculate descriptors at the grid points.

We first performed a CoMFA analysis on all 37 compounds using a partial least squares (PLS) method with Gasteiger charges.[25] All bisphosphonates were taken to have −1 phosphonate charges (charge scheme A, basically as used in our previous studies).[15−18,35−41] The optimum number of components in the PLS model was found to be seven by examining q^2 values, obtained from the leave-one-out cross-validation procedure with the SAMPLS[42] sampling method. The seven-component CoMFA model gave a correlation coefficient $R^2 = 0.93$, a cross-validated correlation coefficient $q^2 = 0.49$ and an F-test = 51.7, as shown in Table 1, along with the experimental and predicted IC_{50} values. The training set results (experimental pIC_{50} versus computed pIC_{50} values) for these compounds are shown graphically in Figure 5A (in blue).

We next carried out a series of calculations to evaluate the predictive value of the CoMFA analysis. We randomly selected

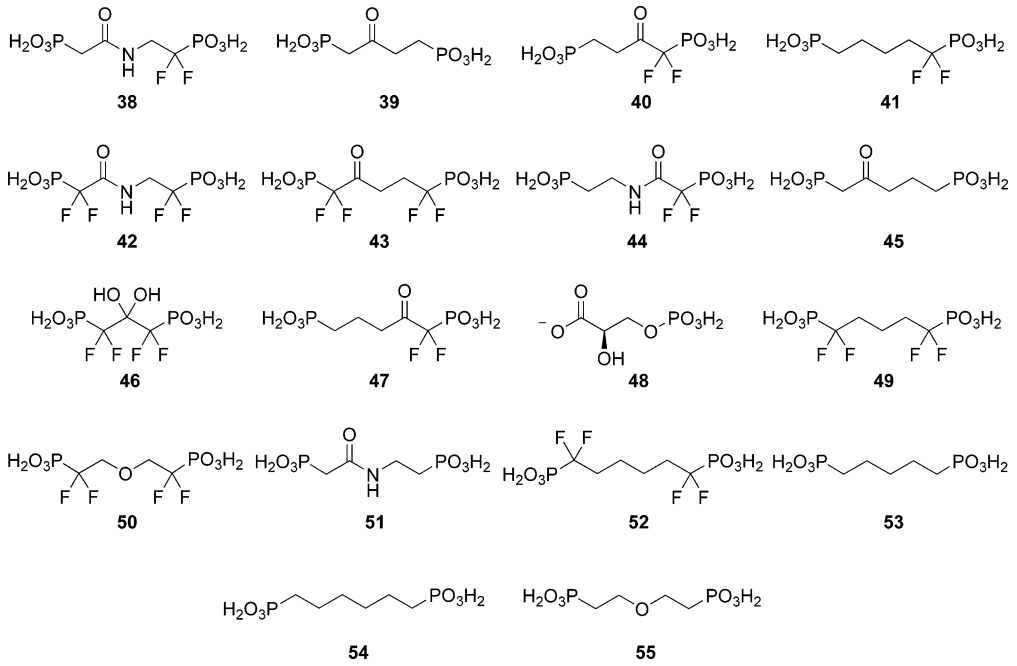

Figure 2. Structures of alkyl bisphosphonates investigated (rank ordered by decreasing activity).

and removed seven compounds from the initial training set, and then a new CoMFA model was computed and the activities of the compounds that had been removed were predicted. The procedure was repeated three more times, generating 28 predicted values. The experimental and predicted pIC_{50} results and their associated statistics, including the external validations (predicted values in boldface type), are shown in Table 1 and graphically in Figure 5A (in red).

While the majority of the predicted pIC_{50} values were close to those found experimentally, the average pIC_{50} error for the 28 predicted values was 0.606 (corresponding to a factor of 4.0 uncertainty in the IC_{50} predictions). There are clearly at least five outliers that degrade the overall correlation. On the basis of the results described in refs 7 and 9, it seemed likely that the use of the uniform (−1, −1) charge scheme might be inappropriate and that the α-halogenated sites might need to be fully deprotonated. We thus repeated the calculations, this time with this alternative charge scheme (charge scheme B). In this case, the CoMFA analysis provided a model that had $R^2 = 0.98$, $q^2 = 0.97$, and an *F*-test = 584, a major improvement (Figure 5B and Table 2). The external validation procedure showed that this new CoMFA model had an average residual pIC_{50} of 0.150 and could predict the inhibition of PGK within a factor of 1.4 (on average) over the range of activities. These results are clearly considerably more accurate than those obtained by using the alternate charge scheme (Table 1). As noted previously,[7,9] the most active compounds have in general both methylene groups substituted with halogens, the intermediate-activity cluster of compounds have just one methylene substituted with a halogen, while the least active compounds have no halogen substituents on the methylene groups.

We next carried out a CoMSIA analysis of the experimental results, following the procedure outlined above for the CoMFA analysis, using steric, electrostatic and acceptor probes to calculate the CoMSIA indices at the grid points. The CoMSIA alignment and grid were the same as those used in the CoMFA analysis discussed above (Figure 4A). For the training set, with uniform −1 phosphonate charges we obtained a seven-component CoMSIA model with $R^2 = 0.95$, $q^2 = 0.85$, and an *F*-test = 99.3, as shown in Table 1, together with the experimental and predicted IC_{50} values. The training and test set results for these compounds are shown graphically in Figure 5C. Here, we again used four 30-compound training sets to predict the activities of four sets of seven compounds. On average, the error in prediction was about a factor of 2.0, an improvement over that obtained with the corresponding CoMFA analysis. The experimental and predicted pIC_{50} results and their associated statistics, including the external validations (predicted values in boldface type), are shown in Table 1 and graphically in Figure 5C. These results were considerably improved upon when we used the pK_a information to select charges (as described above): $R^2 = 0.98$, $q^2 = 0.94$, and an F-test = 317 (Table 2, Figure 5D). The external validation procedure showed that this CoMSIA model (charge scheme B), with an average residual pIC_{50} of 0.225, could predict the inhibition of PGK within a factor of 1.7 (on average) over the range of activities, compared to the 2.0 error factor obtained for the uniform charge model (charge scheme A), supporting again the validity of using the pK_a-based model. The CoMFA and CoMSIA results were highly correlated ($R^2 = 0.97$) and there was no significant improvement in the correlation with experiment when the CoMFA and CoMSIA results were averaged ($R^2 = 0.95$ versus experiment).

Of course, it must be borne in mind that the pK_a information we used to guide our QSAR investigations pertain to bisphosphonates in aqueous solution and that all bisphosphonates might in fact dock to the PGK protein in the same protonation state, independent of their pK_a values in solution—a question that cannot at present be resolved, although in future work it might be possible to deduce this information on the basis of ^{31}P NMR chemical shifts, which are highly sensitive to ionization state.[43] But in any case, the QSAR predictions for these bisphosphonates are quite accurate for both the CoMFA and CoMSIA approaches (with charge scheme B)

We next investigated the CoMSIA field map results from the training set equations. These results are shown in Figure 6 with the steric (Figure 6A), electrostatic (Figure 6B), and acceptor (Figure 6C) field features superimposed on the structure of **1**, the most active compound. The favored steric field feature (green, Figure 6A) clearly encompasses the two methyl groups of the benzene ring and correlates well with the increased

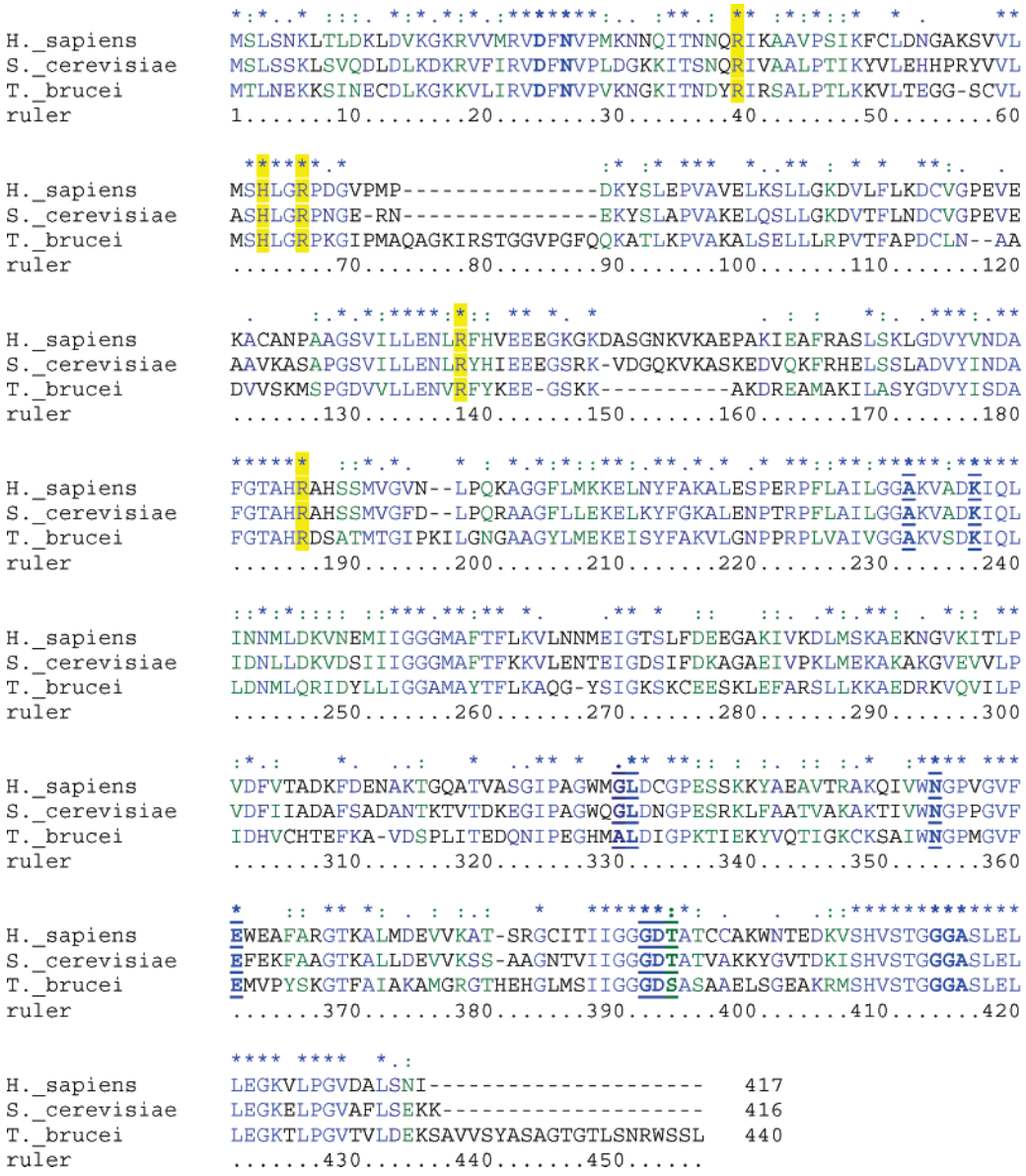

Figure 3. Alignment of human, *S. cerevisiae*, and *T. brucei* phosphoglycerate kinase sequences. The yellow bars indicate highly conserved residues in the "basic patch", thought to interact with 1,3-BPG substrate and the bisphosphonate inhibitors; boldface letters indicate nonbasic residues involved in 3-PGA binding; boldface and underlined letters indicate residues involved in ADP binding.

activity of this substitution pattern, as can be seen in the series **1**−**3** as well as **23**, **24**, **27**, and **37**. The disfavored steric field features (yellow, Figure 6A) map to the phosphonate groups in compounds that have six carbon atoms between the phosphonates, as opposed to the four or five found in the most active species. The electrostatic field feature, as expected, places a negative charge region (red) over each phosphonate group (Figure 6B) since the most active compounds are the ones with fully deprotonated phosphonates. An electrostatic field feature favoring positive charge (blue) is located in the pyridyl nitrogen position in some compounds. Since a pyridyl nitrogen is more electronegative than is a carbon in a benzene ring, this field feature explains the lower activity of each of the N-containing bisphosphonates when compared to their carbon-containing counterparts. Finally, a large favorable hydrogen-bond acceptor feature (magenta, Figure 6C) is found to overlap the halogen site of one (but not both) of the α-substituted carbons. Given the rather symmetric nature of the steric and electrostatic field features seen in Figure 6A,B, this result might at first appear surprising but is of course due to the fact that species such as **13** have (within experimental error) the same activity as do the symmetric tetra- and dihalogen-substituted species (e.g., **1**−**5**). The presence of this feature is also consistent with the importance of isopolar mimicry with the anhydride oxygen in 1,3-BPG, with both the anhydride oxygen and the dihalomethylene groups acting as acceptor groups.

Finally, we investigated the chemical features responsible for PGK inhibition by the aromatic bisphosphonates, with pharmacophore modeling by the Catalyst program.[21] We used the structure/protonation files developed for the CoMFA and CoMSIA analyses to generate a series of Catalyst pharmacophore hypotheses. The top-scoring hypotheses had four features, consisting of two negative ionizable groups (near the bisphosphonates), one hydrophobic feature (near the aromatic ring or the double bond, in **25**), and a halogen feature. The best pharmacophore hypothesis is shown superimposed on **1** in Figure 7A and had an R^2 correlation with activity of 0.93, and the major features seen in the pharmacophore can clearly be correlated with those seen in the CoMSIA fields. More specifically, the negative ionizable pharmacophore features correlate with the negative-charge-favored (red, Figure 6B) electrostatic field features, while the observation of only a single

Table 1. CoMFA and CoMSIA Results for Aryl Bisphosphonates (Charge Scheme A)

	experimental activity		CoMFA predicted pIC_{50}					CoMSIA predicted pIC_{50}				
compd[a]	IC_{50}	pIC_{50}	TS	7-compound test set[b]				TS	7-compound test set[b]			
1	0.84	6.08	6.30	6.19	6.04	6.06	6.34	6.28	6.45	6.10	6.22	6.22
2	0.88	6.06	6.02	**5.67**	6.12	6.15	6.10	6.06	**6.27**	5.78	6.01	6.00
3	0.96	6.02	6.12	**6.16**	6.20	5.93	6.07	6.15	**6.28**	5.84	6.07	6.10
4	0.98	6.01	6.50	6.27	6.33	6.30	**6.33**	6.08	6.10	5.80	6.26	**5.92**
5	1.00	6.00	5.59	5.84	5.57	**5.16**	5.74	5.53	5.64	5.39	**5.35**	5.53
6	1.00	6.00	5.93	6.02	6.03	**4.17**	6.05	5.89	6.13	5.83	**5.70**	5.89
7	1.08	5.97	5.71	5.97	6.13	6.03	**3.81**	5.80	5.85	5.98	5.91	**5.37**
8	1.15	5.94	5.30	5.35	5.79	**4.60**	5.50	6.07	6.06	6.09	**5.91**	5.93
9	1.17	5.93	6.02	**5.85**	5.86	5.83	6.05	6.15	**6.10**	6.36	5.98	6.33
10	1.30	5.89	6.06	5.79	**5.64**	5.96	6.00	5.87	5.89	**5.60**	5.87	5.82
11	1.33	5.88	5.79	5.74	5.60	5.66	5.67	5.86	5.84	6.10	5.75	5.98
12	1.34	5.87	5.69	5.86	5.87	**3.84**	5.61	5.60	5.69	5.92	**5.34**	5.71
13	1.80	5.74	5.46	5.66	5.66	5.56	5.85	5.54	5.57	5.42	5.44	5.76
14	1.98	5.70	5.86	5.78	**5.60**	5.76	5.90	5.32	5.39	**5.15**	5.48	5.30
15	3.60	5.44	5.33	5.52	5.35	5.38	**5.93**	5.59	5.50	5.50	5.49	**5.73**
16	8.00	5.10	5.25	5.21	5.09	5.09	**5.42**	5.15	5.02	5.05	5.03	**5.24**
17	8.35	5.08	4.98	5.03	5.15	5.18	**5.12**	5.16	5.08	5.13	5.12	**5.34**
18	9.40	5.03	4.86	5.15	4.95	5.05	5.06	5.00	5.02	4.69	4.97	4.98
19	10.7	4.97	4.59	**4.43**	4.69	4.65	4.74	4.84	**4.81**	4.70	4.96	4.85
20	16.0	4.80	4.93	5.02	5.01	4.70	4.92	5.04	5.03	5.00	4.90	5.01
21	17.0	4.77	4.81	4.59	4.90	4.80	4.66	4.82	4.80	4.85	4.66	4.75
22	68.8	4.16	3.93	**3.88**	4.02	4.24	4.07	4.23	**4.08**	3.95	4.19	4.35
23	73.0	4.14	4.03	3.95	**3.95**	4.02	3.89	3.87	3.91	**4.23**	3.90	4.00
24	78.0	4.11	4.45	4.18	4.08	**3.43**	4.12	3.71	4.02	4.17	**3.98**	3.81
25	87.0	4.06	3.92	4.07	4.07	4.04	4.16	4.04	3.95	3.44	4.14	4.10
26	89.0	4.05	3.99	3.86	**4.42**	4.10	4.16	4.22	4.12	**3.74**	4.15	4.23
27	99.0	4.00	3.70	**3.60**	3.77	3.92	3.79	3.77	**3.86**	4.02	3.79	3.89
28	102	3.99	4.18	3.96	**4.49**	4.05	4.04	4.05	3.95	**3.84**	3.93	4.00
29	107	3.97	4.05	4.03	3.99	4.00	3.81	3.90	4.06	3.65	4.00	3.82
30	138	3.86	3.89	4.00	3.89	**3.63**	4.02	4.05	3.96	4.32	**3.98**	4.11
31	147	3.83	3.83	3.81	3.90	4.06	**4.38**	4.20	3.93	4.49	4.13	**4.60**
32	150	3.82	3.75	3.68	3.99	3.83	3.89	3.79	3.96	3.70	3.84	3.86
33	163	3.79	4.03	4.04	**4.01**	3.71	3.93	3.62	3.72	**3.89**	3.60	3.74
34	181	3.74	4.41	4.16	**5.66**	3.62	3.87	3.83	3.73	**4.24**	3.91	3.66
35	182	3.74	3.89	3.78	3.78	3.92	**3.82**	4.01	3.85	4.71	3.93	**4.36**
36	193	3.71	3.89	3.61	3.75	**4.00**	3.97	4.03	3.89	4.23	**4.31**	4.08
37	200	3.70	3.95	**4.07**	4.07	3.90	3.83	3.85	**3.85**	4.07	3.83	3.99
$R^{2\,c}$			0.93	0.96	0.97	0.98	0.97	0.95	0.97	0.86	0.97	0.95
$q^{2\,d}$			0.49	0.34	0.71	0.62	0.50	0.85	0.84	0.78	0.80	0.85
F[e]			51.74	63.60	72.74	118.54	72.65	99.32	106.0	48.17	116.6	65.56
N[f]			7	8	8	8	8	6	7	4	7	7
n[g]			37	30	30	30	30	37	30	30	30	30

[a] See Figure 1 for compound structures. [b] Values shown in boldface type represent predicted activities of compounds that were not included in the training set. [c] Average squared correlation coefficient calculated during the validation procedure. [d] Cross-validated correlation coefficient after leave-one-out procedure. [e] Ratio of R^2 explained to unexplained $= R^2/(1 - R^2)$. [f] Optimal number of principal components. [g] Number of compounds.

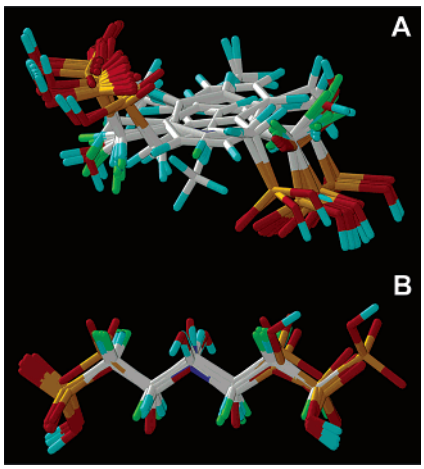

Figure 4. Alignment of compounds: (A) aromatic bisphosphonates and (B) alkyl bisphosphonates (alignment I).

halogen feature (green, Figure 7A) correlates with the single CoMSIA hydrogen-bond acceptor site (purple, Figure 6C).

Alkyl Bisphosphonates. The results described above for the aromatic bisphosphonates show good correlations between the experimental and predicted pIC_{50} values, but the experimental activities clearly fall into three distinct clusters of compounds, having IC_{50} values in the range ~1−4, 8−17, and 69−200 μM (Table 1). The least active species do not contain any halogens; the intermediate-activity species have one halogen, while the most active species contain two or four halogens. As such, there is little chemical diversity. In contrast, the alkyl bisphosphonates are chemically much more diverse and are potentially much more flexible (since none have aromatic rings), making them more challenging from a QSAR perspective. We show in Figure 2 the structures of the 18 alkyl bisphosphonates whose dissociation constants for binding to yeast PGK were reported by Jakeman et al.[8] The experimentally determined dissociation constants (K_d) of compounds **38**−**55** are shown in Table 3 and span over 3 orders of magnitude, from 2 to 5000 μM, an order of magnitude larger range than that seen with the aromatic species. From an initial inspection of the dissociation constants for the different ligands, it is again possible to infer[8] some qualitative structure−activity relationships. First, once again, α-fluorinated compounds show stronger binding to PGK than do their nonfluorinated counterparts, as noted by Jakeman et al.[8] However, with the aliphatic species, the tetrafluorinated

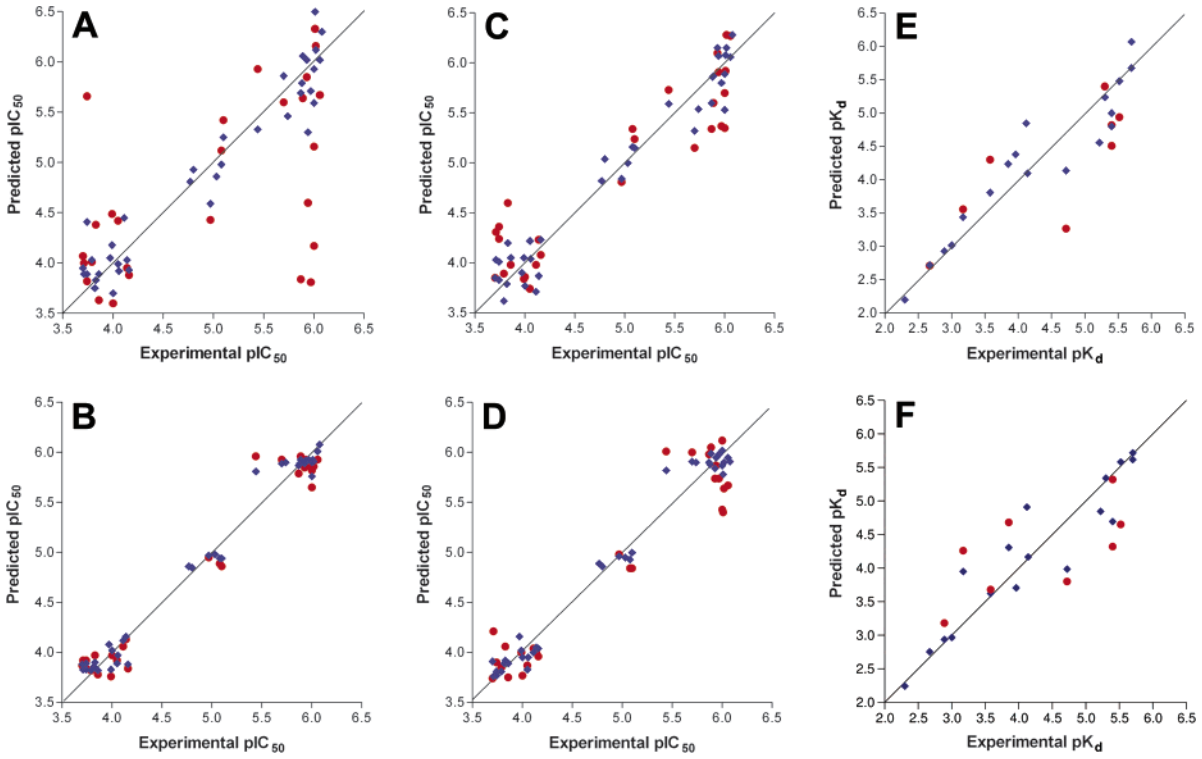

Figure 5. Plots of experimental pIC_{50}/pK_d versus predicted pIC_{50}/pK_d values for the CoMFA and CoMSIA models of aryl bisphosphonates inhibiting human PGK (A−D) and alkyl bisphosphonates inhibiting yeast PGK (E, F). Training set results are shown in blue; test set results are shown in red. (A) Aromatic bisphosphonates, charge scheme A, CoMFA; (B) aromatic bisphosphonates, charge scheme B, CoMFA; (C) aromatic bisphosphonates, charge scheme A, CoMSIA; (D) aromatic bisphosphonates, charge scheme B, CoMSIA; (E) aliphatic bisphosphonates, alignment I, CoMFA; (F) aliphatic bisphosphonates, alignment I, CoMSIA. The lines represent the (ideal) 45° (1:1 correlation) slopes.

bisphosphonates are somewhat less active than are the difluorinated analogues, but the difluorinated compounds are not always more potent than are the nonfluorinated species. This has been proposed to be due to the possibility that if fluorines are on the α-carbon proximal to the carbonyl moiety, the bisphosphonate may bind in an alternate orientation[44] in which the carbonyl has the opposite binding orientation to that seen in 1,3-BPG. Replacement of a methylene group by an oxygen results in a reduction in activity (**53** and **55**), and replacement of a methylene group with a keto group (in the *β* position) in general increases ligand affinity (**45** and **53**), since this type of analogue may better imitate the natural substrate. An amide group, on the other hand, increases activity when compared to an alkyl bisphosphonate, but not to the same extent as does a keto group (**44**, **51**, and **53**). Finally, size matters: four-atom spacers are better than analogous compounds with five-atom spacers (**39** and **45**), and compounds with five-atom spacers are in general better than those with six-atom spacers (**49** and **52**). So, unlike the situation with the aromatic bisphosphonates, whose activity could be readily categorized, this is not possible with the alkyl bisphosphonates and necessitates the use of QSAR methods in order to make predictive structure−activity relationships.

The 18 molecules considered (**37**−**55**), shown in Figure 2, were aligned (Figure 4B, alignment I) with 1,3-BPG as the shape reference and the general orientation (alignment I) proposed by Jakeman et al.[44] More specifically, we used one phosphorus atom and the *β*-carbon for all compounds, except **46**, which was aligned on the basis of the presence of the hydroxyl group and the adjacent carbon of the natural substrate, 1,3-BPG. On the basis of our experience with the aromatic bisphosphonates, protonation states were assigned according to the pK_a values for each molecule and, in general, correlated with the presence or absence of halogens on the α-carbon. All phosphonates adjacent to difluorinated α-carbons were taken to be fully ionized, as were the 3-phosphonate groups of **38**, **45**, and **51** (which have pK_a[3] values < 6). The CoMFA analysis gave a correlation coefficient $R^2 = 0.89$, $q^2 = 0.63$, and an F-test = 19.7, as shown in Table 3, together with the experimental and predicted pK_d values. The training set results for these compounds are shown graphically in Figure 5E. We then evaluated the predictive utility of this model by using reduced training sets ($N = 16$), predicting the activity of the excluded compounds ($N = 2$). The average pK_d error for the eight predicted values, shown in boldface type in Table 3 and graphically in Figure 5E (in red), was 0.61, corresponding to a factor of 4.1 uncertainty in the K_d predictions. To try to improve upon these results, we then carried out a CoMFA analysis using a second alignment (as presented in the early work of Jakeman et al.,[8] alignment II) which has maximal overlap of the common structural features. This model gave, however, $R^2 = 0.82$, $q^2 = 0.29$ and an F-test = 12.6, worse than the results obtained by using alignment I, the more recent published orientation,[44] supporting the validity of alignment I.

Next, we performed a CoMSIA analysis. For the training set based on alignment I, the CoMSIA analysis gave $R^2 = 0.88$, $q^2 = 0.68$, and an F-test = 33.7, as shown in Table 3, together with the experimental and predicted pK_d values. The training set results for these compounds are shown graphically in Figure 5F. The reduced training sets ($N = 16$) gave a 0.58 average pIC_{50} error, corresponding to a factor of 3.8 uncertainty in the IC_{50} predictions for the excluded compounds, shown in boldface type in Table 3 and graphically in Figure 5F (in red). A CoMSIA analysis on alignment II resulted in a model that had $R^2 = 0.8$, $q^2 = 0.48$ and F-test = 21.1, again worse than that obtained by using alignment I. The external validation procedure showed that this CoMSIA model, with an average residual pK_d of 0.67, predicted K_d values with on average a 4.7× error over the range

Table 2. CoMFA and CoMSIA Results for Aryl Bisphosphonates (Charge Scheme B)

	experimental activity		CoMFA predicted pIC_{50}					CoMSIA predicted pIC_{50}				
compd[a]	IC_{50}	pIC_{50}	TS	7-compound test set[b]				TS	7-compound test set[b]			
1	0.84	6.08	6.08	6.06	6.08	6.04	6.11	5.91	5.89	5.87	5.88	6.03
2	0.88	6.06	6.01	**5.93**	6.04	6.01	5.99	5.95	**5.67**	5.99	5.93	5.97
3	0.96	6.02	5.91	**5.86**	5.93	5.88	5.94	5.90	**5.64**	5.93	5.89	5.97
4	0.98	6.01	5.93	5.93	5.96	5.94	**5.86**	5.78	5.86	5.90	6.00	**5.40**
5	1.00	6.00	5.76	5.77	5.75	**5.65**	5.85	5.87	5.95	5.89	**5.43**	5.91
6	1.00	6.00	5.90	5.89	5.93	**5.82**	5.91	6.02	5.98	6.07	**6.12**	5.90
7	1.08	5.97	5.93	5.95	5.97	5.89	**5.88**	5.98	6.04	6.07	5.90	**5.74**
8	1.15	5.94	5.92	5.92	5.96	**5.93**	5.86	5.95	5.96	6.04	**5.87**	5.79
9	1.17	5.93	5.89	**5.85**	5.90	5.85	5.90	5.84	**5.74**	5.81	5.88	5.88
10	1.30	5.89	5.93	5.89	**5.96**	5.90	5.94	5.99	5.78	**6.05**	5.96	6.02
11	1.33	5.88	5.89	5.86	5.91	5.86	5.89	5.88	5.79	5.86	5.92	5.89
12	1.34	5.87	5.87	5.86	5.89	**5.79**	5.87	5.90	5.81	5.90	**5.98**	5.88
13	1.80	5.74	5.90	5.85	5.91	5.87	5.93	5.90	5.85	5.89	5.89	5.99
14	1.98	5.70	5.89	5.89	**5.93**	5.91	5.84	5.91	5.89	**6.00**	5.84	5.80
15	3.60	5.44	5.81	5.78	5.80	5.74	**5.96**	5.82	5.76	5.76	5.76	**6.01**
16	8.00	5.10	4.94	4.93	4.97	4.96	**4.86**	5.00	5.01	5.10	5.05	**4.84**
17	8.35	5.08	4.94	4.92	4.96	4.94	**4.89**	4.93	4.96	4.99	4.93	**4.84**
18	9.40	5.03	4.98	4.98	5.00	4.97	5.00	4.95	5.03	4.90	4.99	4.99
19	10.7	4.97	4.97	**4.95**	4.98	4.99	4.99	4.96	**4.98**	4.91	5.01	5.07
20	16.0	4.80	4.85	4.87	4.81	4.79	4.88	4.86	4.86	4.85	4.71	4.80
21	17.0	4.77	4.86	4.87	4.83	4.80	4.86	4.89	4.86	4.90	4.80	4.81
22	68.8	4.16	3.88	**3.84**	3.87	3.90	3.90	4.04	**3.96**	4.08	4.13	4.04
23	73.0	4.14	4.16	4.16	**4.13**	4.17	4.17	4.05	4.13	**4.00**	4.01	4.13
24	78.0	4.11	4.12	4.13	4.13	**4.06**	4.10	4.00	4.10	3.99	**4.04**	4.00
25	87.0	4.06	3.97	3.98	3.97	3.98	4.04	3.95	3.95	3.92	3.90	3.99
26	89.0	4.05	3.89	3.90	**3.92**	3.93	3.89	3.83	3.88	**3.87**	3.88	3.93
27	99.0	4.00	4.02	**3.97**	4.03	4.05	3.99	3.95	**3.77**	3.96	3.95	4.03
28	102	3.99	3.83	3.84	**3.76**	3.79	3.90	4.02	3.91	**4.00**	3.96	4.01
29	107	3.97	4.08	4.07	4.08	4.07	4.06	4.16	4.09	4.10	4.10	4.15
30	138	3.86	3.82	3.83	3.74	**3.78**	3.92	3.89	3.89	3.79	**3.75**	3.97
31	147	3.83	3.90	3.88	3.87	3.91	**3.97**	3.92	3.95	3.86	3.90	**4.06**
32	150	3.82	3.86	3.82	3.86	3.86	3.86	3.89	3.89	3.96	3.88	3.82
33	163	3.79	3.82	3.79	**3.82**	3.82	3.82	3.81	3.76	**3.85**	3.79	3.79
34	181	3.74	3.89	3.90	**3.92**	3.92	3.89	3.81	3.76	**3.90**	3.85	3.85
35	182	3.74	3.83	3.80	3.83	3.85	**3.84**	3.77	3.74	3.69	3.85	**3.90**
36	193	3.71	3.83	3.82	3.84	**3.92**	3.80	3.76	3.79	3.76	**4.21**	3.68
37	200	3.70	3.88	**3.87**	3.87	3.90	3.93	3.91	**3.74**	3.91	3.91	4.02
R^2[c]			0.98	0.98	0.98	0.98	0.99	0.98	0.98	0.98	0.98	0.99
q^2[d]			0.97	0.97	0.96	0.96	0.98	0.94	0.94	0.93	0.95	0.96
F[e]			584.3	520.0	474.7	433.1	759.6	317.1	290. 5	278.1	262.3	401.9
N[f]			3	3	3	3	3	5	5	5	5	5
n[g]			37	30	30	30	30	37	30	30	30	30

[a] See Figure 1 for compound structures. [b] Values shown in boldface type represent predicted activities of compounds that were not included in the training set. [c] Average squared correlation coefficient calculated during the validation procedure. [d] Cross-validated correlation coefficient after leave-one-out procedure. [e] Ratio of R^2 explained to unexplained $= R^2/(1 - R^2)$. [f] Optimal number of principal components. [g] Number of compounds.

of activities. So, as with the CoMFA analysis, this model is inferior to that obtained by using alignment I.

The CoMSIA field maps obtained by using alignment I are presented in Figure 8 with the steric (Figure 8A), electrostatic (Figure 8B), and acceptor (Figure 8C) field features superimposed on the structure of **38**, the most active aliphatic compound. The unfavorable steric field (yellow) maps onto the phosphonate of this compound, supporting the idea that compounds with four-atom linear chains (**39** and **40**) are generally favored over longer ones (two of the four least active species, **52** and **54**, have six-atom spacer groups). Also, the negative-charge-favored electrostatic field contribution (red, Figure 8B) is adjacent to the α-fluorinated carbon, indicating that difluorination is necessary for increased activity but tetrafluorination is not, especially if it directs the compound to bind in the opposite orientation to 1,3-BPG. And the favorable acceptor field (magenta) overlaps with the oxygen of the amide group, which mimics the carbonyl moiety of the natural substrate.

We also employed the Catalyst program[25] to create a pharmacophore model for bisphosphonate binding to yeast PGK. The pharmacophore model, Figure 7B, is quite similar to that obtained with aromatic bisphosphonate inhibition of the human enzyme. The top-scoring hypothesis (Figure 7B) had five features: three negative ionizable groups (dark blue, near the bisphosphonates) one custom-built hydrophobic feature (cyan), and one custom-built halogen feature (green). The aromatic (Figure 7A) and aliphatic (Figure 7B) pharmacophores are shown superimposed in Figure 7C; however, the aliphatic pharmacophore permitted only a modest correlation with experiment ($R^2 = 0.5$), consistent with the overall poorer performance of the CoMFA and CoMSIA models with the aliphatic bisphosphonates. However, as can be seen in Figures 6 and 8, the CoMSIA fields for both sets of inhibitors clearly do show the importance of a hydrogen-bond acceptor (magenta), important not only for binding orientation but also for tight binding, and the steric fields highlight the fact that the length of the bisphosphonate is also important, most likely because longer bisphosphonates do not fit well into the binding site, due to steric repulsions. The pharmacophore models for both sets of inhibitors also show considerable similarities and emphasize the importance of the negatively charged phosphonate groups, together with the presence in both pharmacophores of a halogen feature close to the α-carbon, which lowers the pK_a of the phosphonate groups, although whether this results in an enhanced electrostatic interaction with the protein mediated via the phosphonate group or whether it reflects primarily the

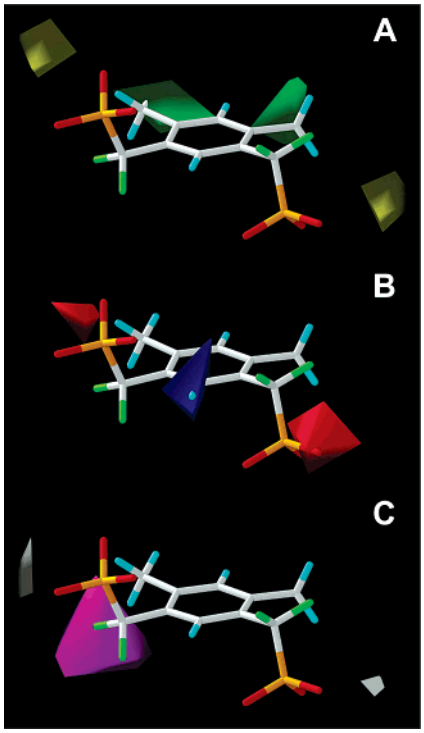

Figure 6. CoMSIA fields for human PGK superimposed on **1**. (A) Steric fields; green indicates steric bulk favorable, yellow indicates steric bulk unfavorable. (B) Electrostatic fields; blue indicates positive charge favorable, red indicates negative charge desirable. (C) Acceptor fields; magenta indicates bond acceptor desirable, white indicates bond acceptor unfavorable.

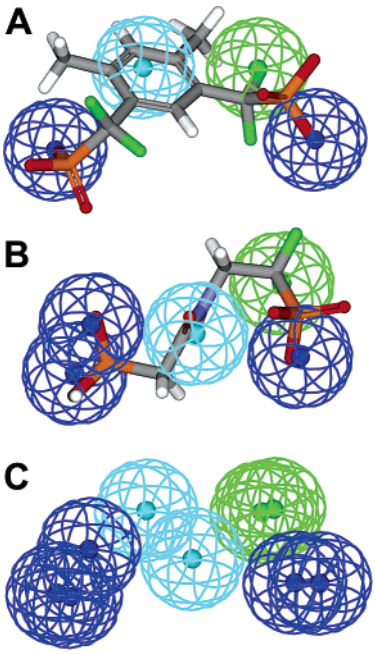

Figure 7. Pharmacophore models for PGK inhibition by bisphosphonates: (A) human PGK inhibition by aromatic bisphosphonates; (B) aliphatic bisphosphonate binding to yeast PGK; (C) superimposed hypotheses (A and B). Blue spheres represent negative ionizable groups, cyan spheres represent hydrophobic features, and green spheres represent halogen features.

ionization (and hence solvation) state of the bisphosphonate in solution remains to be determined.

For yeast PGK, the QSAR results obtained are only about half as accurate as those obtained with the human enzyme. There are several possible reasons for this. First, the data set contains results for only 18 compounds, barely above the minimum number necessary for an accurate QSAR investigation. Second, the dissociation constants were determined indirectly, by measuring the changes in NMR chemical shifts for three histidines in the binding site, and the standard deviations of the measurements for several compounds are relatively large, so there is a larger experimental error in K_d for the yeast PGK than in the human IC_{50} determinations (28% versus 5% errors reported, respectively). Also, of course, the complexities associated with the more flexible nature of the alkyl bisphosphonates may complicate the alignment process and contribute to larger errors, in the case of the yeast enzyme.

Docking Investigations. We next investigated the docking (using AutoDock) of the aromatic compounds **1** and **13** and the best alkyl compound, **38**, to the X-ray crystal structure of the *T. brucei* PGK (PDB file 13PK).[27] PGK is a bilobal protein, composed of two domains connected by a highly conserved hinge region. The C-terminal domain binds the nucleotide MgADP[45] and the N-terminal domain binds 3-PGA.[46] In the open conformation, the two substrates are very far from each other, so a hinge-bending motion mechanism has been postulated to explain how the two substrates come into close proximity and enable phosphoryl transfer to occur. The ternary complex of PGK with 3-PGA, ADP, and Mg^{2+} exhibits such a hinge closure and is believed to be the catalytic conformation; consequently it was used for our docking study. In this structure, the conserved Arg 39, 65, 135, and 172 and His 62 (*T. brucei* PGK numbering; shown in yellow in the sequence alignment in Figure 3) form a "basic patch" (shown in yellow in Figure 9) around 3-PGA, and we used this 3-PGA site for docking of **1**, **13**, and **38**. The lowest energy structure of **1** docked to PGK−ADP−Mg^{2+} is shown in Figure 10A, superimposed on the 3-PGA ligand (in yellow). The rms difference is 1.56 Å when three of the heavy atoms (phosphorus, the adjacent carbon, and the carbon of the carboxylate) of 3-PGA and **1** (phosphorus, the adjacent carbon, and the ring carbon where the difluoromethylene phosphate is attached) are used. In the case of **13** (which contains a single CF_2 group), we obtained two sets of clusters, one in which the CF_2 is next to what would be the transferable phosphate (alignment II) and the other in which the CF_2 group is adjacent to the phosphate group interacting with the basic patch (alignment I).[44] The former cluster had a slightly lower (∼0.5 kcal) energy but was more sparsely populated, while the latter was more densely populated (19 vs 10 structures) and had the expected orientation (alignment I), shown in Figure 10B, corresponding to the more recent proposal of Jakeman et al.[44] The rms deviation between the coordinates of the three heavy atoms (mentioned above) of 3-PGA and **13** in this alignment is 0.400Å. For the best alkyl compound **38**, we again obtained two sets of clusters, following the same pattern seen for **13**. The lowest energy cluster corresponded to alignment II while the more densely populated cluster with slightly lower energy (∼0.18 kcal), in which the difluoromethylene group interacts with the basic patch, corresponded to alignment I. The rms deviation between the coordinates of four heavy atoms (phosphorus, two adjacent carbons, and the carbon of the carboxylate) of 3-PGK and **38** (phosphorus, two adjacent carbons, and the carbon following the NH group) was found to be 0.485 Å (Figure 10C). Since ∼70% of the energetically favored structures correspond to alignment I (in which the αF_2 groups can interact with the basic patch) and since this alignment gives the best results in the QSAR calculations, the preponderance of the evidence supports this binding mode (the recent Jakeman et al.[44] proposal) to PGK.

Table 3. CoMFA and CoMSIA Results for Alkyl Bisphosphonates (Alignment I)

	experimental activity		CoMFA predicted pK_d					CoMSIA predicted pK_d				
compd[a]	K_d	pK_d	TS	2-compound test set[b]				TS	2-compound test set[b]			
38	2	5.70	5.68	5.64	5.26	5.57	5.50	5.72	5.83	5.42	5.73	5.63
39	2	5.70	6.07	5.81	5.82	5.77	5.81	5.62	5.74	5.50	5.42	5.53
40	3	5.52	5.48	5.50	5.69	**4.94**	5.46	5.58	5.51	5.40	**4.65**	5.63
41	4	5.40	5.00	5.12	**4.82**	5.15	5.25	4.69	4.62	**4.32**	4.66	4.88
42	4	5.40	4.80	4.94	4.69	**4.51**	4.86	5.32	5.46	5.36	**5.32**	5.42
43	5	5.30	5.24	5.17	4.88	4.92	5.25	5.34	5.44	5.36	5.38	5.45
44	6	5.22	4.56	5.00	4.87	4.90	4.96	4.85	4.83	4.69	4.86	4.87
45	19	4.72	4.14	3.87	**3.27**	3.96	3.99	3.98	4.26	**3.80**	4.06	3.97
46	72	4.14	4.10	3.71	3.97	3.67	3.73	4.17	4.12	4.24	4.26	4.16
47	76	4.12	4.85	5.14	4.98	5.22	5.26	4.91	4.88	4.73	4.95	4.93
48	110	3.96	4.38	4.01	4.07	4.03	3.99	3.71	3.69	3.66	3.76	3.77
49	140	3.85	4.24	4.52	4.31	4.20	**4.68**	4.31	4.27	4.27	4.26	**4.68**
50	256	3.58	3.81	**4.30**	4.12	3.75	4.21	3.62	**3.68**	3.73	3.51	3.76
51	675	3.17	3.44	**3.56**	3.01	3.35	3.33	3.95	**4.26**	3.78	3.99	3.92
52	1000	3.00	3.02	3.03	3.08	3.03	3.05	2.97	2.96	3.03	2.97	3.04
53	1300	2.89	2.93	3.04	2.62	3.05	**3.29**	2.94	3.06	2.69	2.92	**3.18**
54	2130	2.67	2.72	2.68	2.74	2.84	2.69	2.75	2.77	2.54	2.82	2.71
55	5000	2.30	2.20	2.70	2.43	2.33	2.56	2.24	2.46	2.14	2.17	2.26
R^2[c]			0.89	0.86	0.88	0.86	0.85	0.88	0.91	0.93	0.85	0.88
q^2[d]			0.63	0.49	0.64	0.45	0.51	0.68	0.67	0.73	0.57	0.64
F[e]			19.74	15.96	20.54	17.48	15.96	33.71	39.27	80.13	22.83	30.35
N[f]			5	4	4	4	4	3	3	2	3	3
n[g]			18	16	16	16	16	18	16	16	16	16

[a] See Figure 2 for compound structures. [b] Values shown in boldface type represent predicted activities of compounds that were not included in the training set. [c] Average squared correlation coefficient calculated during the validation procedure. [d] Cross-validated correlation coefficient after leave-one-out procedure. [e] Ratio of R^2 explained to unexplained $= R^2/(1 - R^2)$. [f] Optimal number of principal components. [g] Number of compounds.

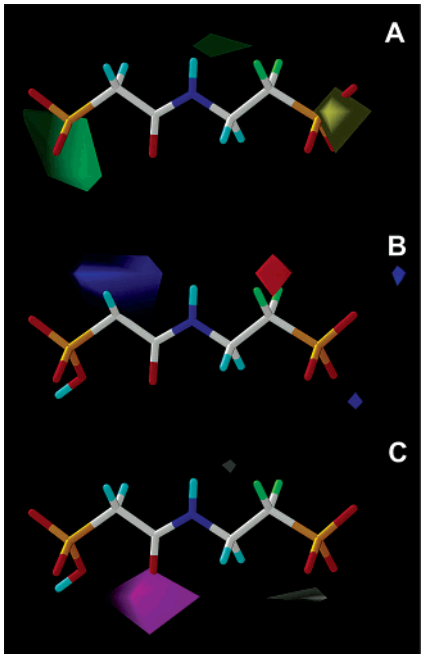

Figure 8. CoMSIA fields for yeast PGK inhibition by aliphatic bisphosphonates. (A) Steric fields; green indicates steric bulk favorable, yellow indicates steric bulk unfavorable. (B) Electrostatic fields; blue indicates positive charge favorable, red indicates negative charge favorable. (C) Acceptor fields; magenta indicates hydrogen-bond acceptor favorable, white indicates hydrogen-bond acceptor unfavorable.

Of course, the possibility exists that better results might be obtained by using the protein crystal structures for the *S. cerevisiae* and *H. sapiens* enzymes. However, the *S. cerevisiae* protein is in the "open" conformation and initial docking attempts were not successful, and there is no reported structure for the human protein. We therefore constructed homology models for both the *S. cerevisiae* and *H. sapiens* proteins using the *T. brucei* structure as a template, basically as described previously for FPPS.[47] The results so obtained are shown in the Supporting Information, Figures S1 and S2, for **1**, **13**, and **38** bound to the *H.* sapiens (Figure S1) and *S. cerevisiae* (Figure S2) homology models. The rms deviation between the crystallographic (3-PGA, three heavy atoms, *T. brucei*) and docked structures (determined as described above) was found to be 1.69 (±0.42) Å, about twice the 0.82 Å average value seen in the *T. brucei* comparison. Nevertheless, the overall docked poses (Figures 10, S1, and S2) are clearly very similar to those discussed in detail for *T. brucei*, and the pharmacophores and CoMSIA field features can be readily superimposed on these poses, as shown for example in Figure S3 in the Supporting Information.

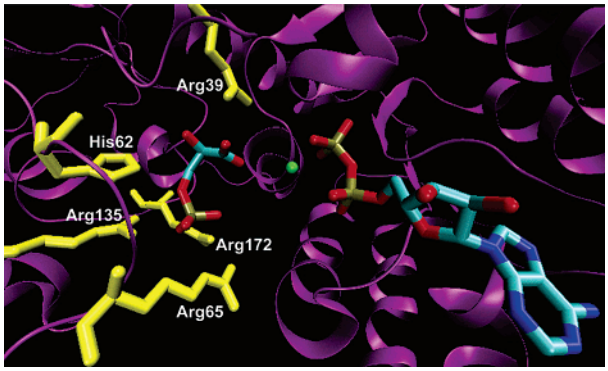

Figure 9. *T. brucei* PGK binding site with basic patch residues shown in yellow; 3-PGA is shown on the left, with ADP on the right and Mg^{2+} (center) in green.

Conclusions

The results we have presented above are of interest for several reasons. First, they provide the first quantitative analysis of the inhibition of human phosphoglycerate kinase by aromatic bisphosphonates by 3D-QSAR (CoMFA, CoMSIA) and pharmacophore modeling methods. Good results were obtained by using both CoMFA and CoMSIA methods, with the latter having the advantage of providing graphical information on the importance of steric, electrostatic, and hydrogen-bond acceptor

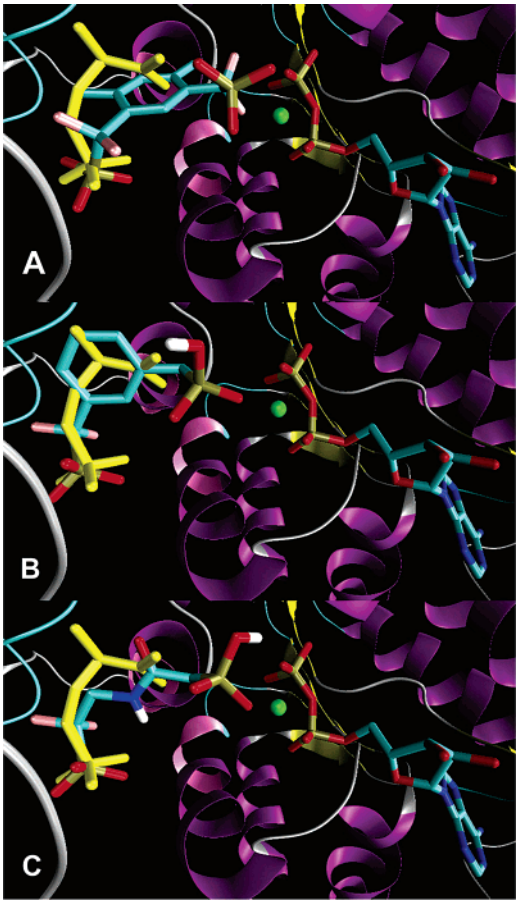

Figure 10. AutoDock structures of (A) **1**, (B) **13**, and (C) **38**, docked to a closed-conformation *T. brucei* PGK. All structures are shown superimposed on 3-PGA, in yellow. ADP is shown on the right; Mg^{2+} (center) is shown in green. The structures shown in panels B and C are the most populous low-energy ones.

features for activity. Second, we report the first quantitative analysis of the binding of alkyl bisphosphonates to yeast PGK, with activities being predicted within, on average, a factor of 4 over a 2500× overall range in activity. For both sets of inhibitors, hydrogen-bond acceptor features (corresponding to the carboxylate group and anhydride oxygen in the native 1,3-BPG substrate) were detected, together with additional steric and hydrophobic field features associated with the spacer region between the phosphonate groups. Third, we used pharmacophore modeling to investigate both sets of inhibitors. Both pharmacophores contained negative ionizable features (phosphonates), a steric feature corresponding to the ring or the aliphatic chain between the phosphonates, and a halogen feature. And finally, we used a computational docking (AutoDock) method to investigate the docking of both aromatic and aliphatic bisphosphonates to the *T. brucei* PGK. These results showed that the most highly populated low-energy conformers corresponded to the most recently proposed alignment,[44] the one that also permitted the most accurate activity predictions with the more challenging, alkyl bisphosphonates. Given that PGK inhibitors are of interest as targets for novel antiparasitic drugs, in addition to being of interest in the context of the treatment of cardiovascular disease,[4,5] together with the fact that several crystallographic structures of PGKs are now available, these results can all be expected to help guide the development of other novel, specific inhibitors of this important glycolytic enzyme.

Acknowledgment. This work was supported by the U.S. Public Health Service (NIH Grant GM073216 to E.O.). G.S. was supported by an NIH Institutional NRSA in Molecular Biophysics Training Grant (GM-08276).

Supporting Information Available: Figures showing docked poses and pharmacophore models. This material is available free of charge via the Internet at http://pubs.acs.org.

References

(1) Bressi, J. C.; Choe, J.; Hough, M. T.; Buckner, F. S.; Van Voorhis, W. C.; Verlinde, C. L. M. J.; Hol, W. G. J.; Gelb, M. H. Adenosine analogues as inhibitors of *Trypanosoma brucei* phosphoglycerate kinase: Elucidation of a novel binding mode for a 2-amino-N6-substituted adenosine. *J. Med. Chem.* **2000**, *43*, 4135−4150.

(2) Bakker, B. M.; Michels, P. A. M.; Opperdoes, F. R.; Westerhoff, H. V. Glycolysis in bloodstream form *Trypanosoma brucei* can be understood in terms of the kinetics of the glycolytic enzymes. *J. Biol. Chem.* **1997**, *272*, 3207−3215.

(3) Bakker, B. M.; Michels, P. A. M.; Opperdoes, F. R.; Westerhoff, H. V. What controls glycolysis in bloodstream form *Trypanosoma brucei*. *J. Biol. Chem.* **1998**, *274*, 14551−14559.

(4) Bellingham, A. J.; Detter, J. C.; Lenfant, C. Regulatory mechanisms of hemoglobin oxygen affinity in acidosis and alkalosis. *J. Clin. Invest.* **1971**, *50*, 700−706.

(5) Benesch, R. E.; Benesch, R.; Yu, C. I. The oxygenation of hemoglobin in the presence of 2,3-diphosphoglycerate. Effect of temperature, pH, ionic strength, and hemoglobin concentration. *Biochemistry* **1969**, *8*, 2567−2571.

(6) McHarg, J.; Littlechild, J. A. Studies with inhibitors of the glycolytic enzyme phosphoglycerate kinase for potential treatment of cardiovascular and respiratory disorders. *J. Pharm. Pharmacol.* **1996**, *48*, 201−205.

(7) Caplan, N. A.; Pogson, C. I.; Hayes, D. J.; Blackburn G. M. Novel bisphosphonate inhibitors of phosphoglycerate kinase. *Bioorg. Med. Chem. Lett.* **1998**, *8*, 515−520.

(8) Jakeman, D. L.; Ivory, A. J.; Williamson, M. P.; Blackburn, G. M. Highly potent bisphosphonate ligands for phosphoglycerate kinase. *J. Med. Chem.* **1998**, *41*, 4439−4452.

(9) Caplan, N. A.; Pogson, C. I.; Hayes, D. J.; Blackburn, G. M. The synthesis of novel bisphosphonates as inhibitors of phosphoglycerate kinase (3-PGK). *J. Chem. Soc., Perkin Trans. 1* **2000**, *3*, 421−437.

(10) Blackburn, G. M.; England, D. A.; Kolkmann, F. Monofluoro- and difluoro-methylenebisphosphonic acids: isopolar analogues of pyrophosphoric acid. *J. Chem. Soc., Chem. Commun.* **1981**, 930−932.

(11) Thatcher, G. R. J.; Campbell, A. S. Phosphonates as mimics of phosphate biomolecules: ab initio calculations on tetrahedral ground states and pentacoordinate intermediates for phosphoryl transfer. *J. Org. Chem.* **1993**, *58*, 2272−2281.

(12) Yardley, V.; Khan, A. A.; Martin, M. B.; Slifer, T. R.; Araujo, F. G.; Moreno, S. N.; Docampo, R.; Croft, S. L.; Oldfield, E. In vivo activities of farnesyl pyrophosphate synthase inhibitors against *Leishmania donovani* and *Toxoplasma gondii*. *Antimicrob. Agents Chemother.* **2002**, *46*, 929−931.

(13) Rodriguez, N.; Bailey, B. N.; Martin, M. B.; Oldfield, E.; Urbina, J. A.; Docampo, R. Radical cure of experimental cutaneous leishmaniasis by the bisphosphonate pamidronate. *J. Infect. Dis.* **2002**, *186*, 138−140.

(14) Martin, M. B.; Grimley, J. S.; Lewis, J. C.; Heath, H. T., 3rd; Bailey, B. N.; Kendrick, H.; Yardley, V.; Caldera, A.; Lira, R.; Urbina, J. A.; Moreno, S. N.; Docampo, R.; Croft, S. L.; Oldfield, E. Bisphosphonates inhibit the growth of *Trypanosoma brucei*, *Trypanosoma cruzi*, *Leishmania donovani*, *Toxoplasma gondii*, and *Plasmodium falciparum*: a potential route to chemotherapy. *J. Med. Chem.* **2001**, *44*, 909−916.

(15) Martin, M. B.; Sanders, J. M.; Kendrick, H.; de Luca-Fradley, K.; Lewis, J. C.; Grimley, J. S.; Van Brussel, E. M.; Olsen, J. R.; Meints, G. A.; Burzynska, A.; Kafarski, P.; Croft, S. L.; Oldfield, E. Activity of bisphosphonates against *Trypanosoma brucei rhodesiense*. *J. Med. Chem.* **2002**, *45*, 2904−2914.

(16) Sanders, J. M.; Gomez, A. O.; Mao, J.; Meints, G. A.; Van Brussel, E. M.; Burzynska, A.; Kafarski, P.; Gonzalez-Pacanowska, D.; Oldfield, E. 3-D QSAR investigations of the inhibition of *Leishmania major* farnesyl pyrophosphate synthase by bisphosphonates. *J. Med. Chem.* **2003**, *46*, 5171−5183.

(17) Sanders, J. M.; Song, Y.; Chan, J. M.; Zhang, Y.; Jennings, S.; Kosztowski, T.; Odeh, S.; Flessner, R.; Schwerdtfeger, C.; Kotsikorou, E.; Meits, G. A.; Gomez, A. O.; Gonzalez-Pacanowska, D.; Raker, A. M.; Wang, H.; van Beek, E. R.; Papapoulos, S. E.; Morita, C. T.; Oldfield, E. Pyridinium-1-yl bisphosphonates are potent inhibitors of farnesyl diphosphate synthase and bone resorption. *J. Med. Chem.* **2005**, *48*, 2957−2963.

(18) Hudock, M. P.; Sanz-Rodriguez, C. E.; Song, Y.; Chan, J. M.; Zhang, Y.; Odeh, S.; Kosztowski, T.; Leon-Rossell, A.; Concepcion, J. L.; Yardley, V.; Croft, S. L.; Urbina, J. A.; Oldfield, E. Inhibition of *Trypanosoma cruzi* hexokinase by bisphosphonates. *J. Med. Chem.* **2006**, *49*, 215−223.
(19) Cramer, R. D., 3rd; Patterson, D. E.; Bunce, J. D. Recent advances in comparative molecular field analysis (CoMFA). *Prog. Clin. Biol. Res.* **1989**, *291*, 161−165.
(20) Klebe, G.; Abraham, U.; Mietzner, T. Molecular similarity indices in a comparative analysis (CoMSIA) of drug molecules to correlate and predict their biological activity. *J. Med. Chem.* **1994**, *37*, 4130−4146.
(21) Accelrys. *Catalyst 4.8*; Accelrys Inc.: San Diego, CA.
(22) Tripos. *SYBYL 7.0*; Tripos Inc.: St. Louis, MO**.**
(23) Powell, M. J. D. Restart procedures of the conjugate gradient method. *Math Programming* **1977**, *12*, 241−254.
(24) Press, W. H. *Numerical recipes in C: the art of scientific computing*; Cambridge University Press: New York, 1988; p 324.
(25) Gasteiger, J.; Marsili, M. Iterative partial equalization of orbital electronegativity−rapid access to atomic charges. *Tetrahedron* **1980**, *36*, 3219−3228.
(26) Coodsell, D. S.; Morris, G. M.; Olson, A. J. Automated docking of flexible ligands: applications of AutoDock. *J. Mol. Recognit.* **1996**, *9*, 1−5.
(27) Bernstein, B. E.; Michels, P. A.; Hol, W. G. Synergistic effects of substrate-induced conformational changes in phosphoglycerate kinase activation. *Nature* **1997**, *385*, 275−278.
(28) Cheng, F.; Oldfield, E. Inhibition of isoprene biosynthesis pathway enzymes by phosphonates, bisphosphonates, and diphosphates. *J. Med. Chem.* **2004**, *47*, 5149−5158.
(29) Hosfield, D. J.; Zhang, Y.; Dougan, D. R.; Brown, A.; Tari, L. W.; Swanson, R. V.; Finn, J. Structural basis for bisphosphonate-mediated inhibition of isoprenoid biosynthesis. *J. Biol. Chem.* **2004**, *279*, 8526−8529.
(30) Gabelli, S. B.; McLellan, J. S.; Montalvetti, A.; Oldfield, E.; Docampo, R.; Amzel, L. M. Structure and mechanism of the farnesyl diphosphate synthase from *Trypanosoma cruzi*: implications for drug design. *Proteins: Struct., Funct., Bioinf.* **2006**, *62*, 80−88.
(31) Rondeau, J.; Bitsch, F.; Bourgier, E.; Geiser, M.; Hemmig, R.; Kroemer, M.; Lehmann, S.; Ramage, P.; Rieffel, S.; Strauss, A.; Green, J. R.; Jahnke, W. Structural basis for the exceptional in vivo efficacy of bisphosphonate drugs. *Chem. Med. Chem.* **2006**, *1*, 267−273.
(32) (a) Kavanagh, K. L.; Guo, K.; Wu, X.; Von Delft, F.; Arrowsmith, C.; Sundstrom, M.; Edwards, A.; Opperman, U. X-ray structure of farnesyl diphosphate synthase protein, PDB file 1ZW5. (b) Kavanagh, K. L.; Guo, K.; Von Delft, F.; Arrowsmith, C.; Sundstrom, M.; Edwards, A.; Opperman, U. Human farnesyl diphosphate synthase complexed with Mg and risedronate, PDB file 1YV5.
(33) Szilagyi, A. N.; Ghosh, M.; Garman, E.; Vas, M. A 1.8 Å resolution structure of pig muscle 3-phosphoglycerate kinase with bound MgADP and 3-phosphoglycerate in open conformation: new insight into the role of the nucleotide in domain closure. *J. Mol. Biol.* **2001**, *306*, 499−511.
(34) Watson, H. C.; Walker, N. P.; Shaw, P. J.; Bryant, T. N.; Wendell, P. L.; Fothergill, L. A.; Perkins, R. E.; Conroy, S. C.; Dobson, M. J.; Tuite, M. F.; Kingsman, A. J.; Kingsman, S. M. Sequence and structure of yeast phosphoglycerate kinase. *EMBO J.* **1982**, *1*, 1635−1640.
(35) Szabo, C. M.; Oldfield, E. An investigation of bisphosphonate inhibition of a vacuolar proton-pumping pyrophosphatase. *Biochem. Biophys. Res. Commun.* **2001**, *287*, 468−473.
(36) Szabo, C. M.; Matsumura, Y.; Fukura, S.; Martin, M. B.; Sanders, J. M.; Sengupta, S.; Cieslak, J. A.; Loftus, T. C.; Lea, C. R.; Lee, H. J.; Koohang, A.; Coates, R. M.; Sagami, H.; Oldfield, E. Inhibition of geranylgeranyl diphosphate synthase by bisphosphonates and diphosphates: a potential route to new bone antiresorption and antiparasitic agents. *J. Med. Chem.* **2002**, *45*, 2185−2196.
(37) Szabo, C. M.; Martin, M. B.; Oldfield, E. An investigation of bone resorption and *Dictyostelium discoideum* growth inhibition by bisphosphonate drugs. *J. Med. Chem.* **2002**, *45*, 2894−2903.
(38) Kotsikorou, E.; Oldfield, E. A quantitative structure−activity relationship and pharmacophore modeling investigation of aryl-X and heterocyclic bisphosphonates as bone resorption agents. *J. Med. Chem.* **2003**, *46*, 2932−2944.
(39) Sanders, J. M.; Ghosh, S.; Chan, J. M.; Meints, G.; Wang, H.; Raker, A. M.; Song, Y.; Colantino, A.; Burzynska, A.; Kafarski, P.; Morita, C. T.; Oldfield, E. Quantitative structure−activity relationships for γδ T cell activation by bisphosphonates. *J. Med. Chem.* **2004**, *47*, 375−384.
(40) Ling, Y.; Sahota, G.; Odeh, S.; Chan, J. M.; Araujo, F. G.; Moreno, S. N.; Oldfield, E. Bisphosphonate inhibitors of *Toxoplasma gondii* growth: in vitro, QSAR, and in vivo investigations. *J. Med. Chem.* **2005**, *48*, 3130−3140.
(41) Kotsikorou, E.; Song, Y.; Chan, J. M.; Faelens, S.; Tovian, Z.; Broderick, E.; Bakalara, N.; Docampo, R.; Oldfield, E. Bisphosphonate inhibition of the exopolyphosphatase activity of the *Trypanosoma brucei* soluble vacuolar pyrophosphatase. *J. Med. Chem.* **2005**, *48*, 6128−6139.
(42) Bush, B. L.; Nachbar, R. B., Jr. Sample-distance partial least squares: PLS optimized for many variables, with application to CoMFA. *J. Comput.-Aided Mol. Des.* **1993**, *7*, 587−619.
(43) Burt, C. T. *Phosphorus NMR in Biology*; CRC Press: Boca Raton, FL, 1987.
(44) Jakeman, D. L.; Ivory, A. J.; Blackburn, G. M.; Williamson, M. P. Orientation of 1,3-bisphosphoglycerate analogues bound to phosphoglycerate kinase. *J. Biol. Chem.* **2003**, *278*, 10957−10962.
(45) Davies, G. J.; Gamblin, S. J.; Littlechild, J. A.; Dauter, Z.; Wilson, K. S.; Watson, H. C. Structure of the ADP complex of the 3-phosphoglycerate kinase from *Bacillus stearothermophilus* at 1.65 Å. *Acta Crystallogr.* **1994**, *D50*, 202−209.
(46) Harlos, K.; Vas, M.; Blake, C. F. Crystal structure of the binary complex of pig muscle phosphoglycerate kinase and its substrate 3-phospho-D-glycerate. *Proteins: Struct., Funct., Genet.* **1992**, *12*, 133−144.
(47) Montalvetti, A.; Fernandez, A.; Sanders, J. M.; Ghosh, S.; van Brussel, E.; Oldfield, E.; Docampo, R. Farnesyl Pyrophosphate Synthase Is an Essential Enzyme in *Trypanosoma brucei*. *J. Biol. Chem.* **2003**, *278*, 17075−17083.

JM0604833